

# Shear-thickening of dense bidispersed suspensions

Alessandro Monti<sup>1\*</sup>† and Marco Edoardo Rosti<sup>1\*</sup>†

<sup>1\*</sup>Complex Fluids and Flows Unit, Okinawa Institute of Science and Technology, 1919-1 Tancha, Onna, Kunigami District, 904-0495, Okinawa, Japan.

\*Corresponding author(s). E-mail(s): [alessandro.monti@oist.jp](mailto:alessandro.monti@oist.jp); [marco.rosti@oist.jp](mailto:marco.rosti@oist.jp);

†These authors contributed equally to this work.

## Abstract

We study the rheological behaviour of a dense bidispersed suspension varying the relative size of the two dispersed phases. The main outcome of our analysis is that an enhanced flowability (reduced relative viscosity) of the suspension can be achieved by increasing the dispersion ratio of the phases. We explain the observed result by showing that the presence of large particles increases the packing efficiency of the suspension, leading to a reduction of the contribution of the contacts on the overall viscosity of the suspension in the shear-thickening regime, i.e. where the contacts are the dominating component.

**Keywords:** Shear-thickening, Dense suspensions, Dispersion ratio, Packing

## 1 Introduction

Dense suspensions of rigid, spherical particles immersed in a Newtonian fluid tend to exhibit a lower flowability, acting almost like a rigid solid when subjected to an increasing shear stress. This behaviour, which is well-known in the framework of non-Newtonian fluids, undergoes the name of shear-thickening [2, 16, 34, 35, 45]. Shear-thickening suspensions are becoming increasingly important in industry, with preferential applications in shock absorbers, such as soft-body armours, or into smart fluids with rheological properties that can be tuned by acting on the mechanisms of the stress transmission [10, 28, 38]. The growing relevance of such fluids has stimulated the recent progress made to unravel the mechanisms that dominate the thickening behaviour. In particular, simulations and experiments have shown that, when an increasing stress that exceeds a critical value is applied to a dense

suspension, the rheological response due to the interacting particles switches from mainly lubricative to chains of frictionally contacting grains that transmit the stress and reduce the flowability of the suspension [14, 19, 27, 42, 46]. Shear thickening has been classified into two regimes, named after the macroscopic behaviour of the dense suspensions: continuous shear thickening (CST), i.e. identifiable as a smooth increase of the viscosity with the shear rate, and discontinuous shear thickening (DST), i.e. an abrupt transition to a solid-like suspension with reduced flowability [5, 6, 14, 33, 42]. The two behaviours have been observed for several kinds of dense suspensions that span from monodisperse to polydisperse in terms of size of the beads [11, 31, 41], and made of Brownian [2, 33] or non-Brownian particles [26, 32, 36, 46].

Considering bidispersed suspensions, several parameters can be used to control the shear-thickening regime. Surely, one of those is the

friction coefficient of the particles, that can be tuned to increase or reduce the viscosity in the thickened regime [23, 24, 37, 40]. Among the other parameters, the dispersion ratio and the relative percentage of volume fraction of the two dispersed phases can also be used to modify the shear-thickening behaviour [3, 25, 30, 31]. However, within the literature, there are interpretation of experimental results that look in contrast with the theory of maximally random jammed (MRJ) packings [13, 44] and of the densest binary sphere packings [21, 22]. The latter show that adding particles of different sizes is a more efficient way of packing particles, with an increased MRJ packing, thus suggesting, in the case of flowing suspensions, an increased flowability and a postponement of the onset (critical value of the stress) of the DST when gradually enhancing the total volume fraction of the suspension. This was also observed by D’Haene and Mewis [12], who characterized the rheological behaviour of bimodal colloidal suspensions. On the other side, recent experimental studies [30, 31] show that, by adding an increasing volume fraction of large particles, the suspension can be successfully led to a transition from CST to DST, thus resulting in a larger suspension viscosity at a fixed shear rate in the presence of large particles. The authors proposed a geometrical explanation based on an excluded-volume effect to justify the experimental observations: the presence of large particles causes the formation of shells around them (with size linked to the radius of the small ones), mostly composed of aqueous solution since the small beads are hindered of densely packing around a large sphere, resulting in a local decrease of the concentration of the small particles within the volume of the shells. This local decrease of volume fraction is compensated by an increased concentration in other regions of the suspension, due to mass-conservation, that triggers the discontinuous thickening [30, 31].

In this work, we reconcile the apparent contradiction between the literature data on the subject by showing that the suspension viscosity reduces when mixing large particles in a suspensions at a fixed total volume fraction and shear rate. As a consequence, we show that a dense bidispersed suspension with large dispersion size exhibits a milder shear thickening regime compared to a suspension having identical volume fraction and a lower dispersion ratio, consistent with the higher

efficiency of the MRJ packing shown by the highly bidispersed suspensions [22]. Studies on the effect of the particles sizes were carried out in the past [7–9, 39]. These works numerically tackled the effect of bidispersion by varying the dispersion size and the relative volume ratio between the large and small dispersed particles. A decrease in viscosity has been recorded as the suspension moved from monodisperse to bidispersed, with a minimum taking place when the  $\phi_2/\phi = 0.65$ , where  $\phi_2$  is the volume fraction of the large dispersed phase and  $\phi$  is the volume fraction of the suspension [39]. A further decrease in viscosity has been observed when the dispersion ratio increases, i.e. increasing the size of the larger dispersed phase compared to the smaller one [39]. The suspensions studied in those works, however, contained a relatively small number of particles  $n \leq 2000$ , and no variation of the shear-rate has been included. Here, we extend the previous studies by increasing the number of particles of the suspensions and by introducing the shear-rate dependency, specifically studying the effect of bidispersion on the shear-thickening.

## 2 Methodology

The problem at hand has been tackled by numerically investigating the effects on the shear-thickening region for three configurations of bidispersed suspensions of frictional particles subjected to a uniform shear-flow, with dispersion size  $\lambda = a_2/a_1$  in the range  $\{1.5, 3.0, 6.0\}$  ( $a_1$  and  $a_2$  being the radius of the small and large suspended phase, respectively). The total number of particles is set to  $n = 2^{16}$ , with the number of particles of the two dispersed phases determined by fixing the relative volume between them equal to  $V_2/V_1 = 0.25$ ; four total volume fractions of the suspension are considered:  $\phi = \{0.45, 0.50, 0.55, 0.60\}$ . To extend the validity of the results, for the suspension with  $\phi = 0.60$ , we considered three relative volumes of the dispersed phases, such that  $\phi_2/\phi = \{0.2, 0.5, 0.8\}$ , where  $\phi_2$  is the volume fraction of the larger phase. Figure 1 shows a representation of the three dispersion sizes considered, with the larger phase highlighted with a colour-scheme that will be kept through the whole manuscript.

The numerical investigation is carried out using a validated and publicly available software, *CFF-Ball-0x* [36]. *CFF-Ball-0x* is an in-house

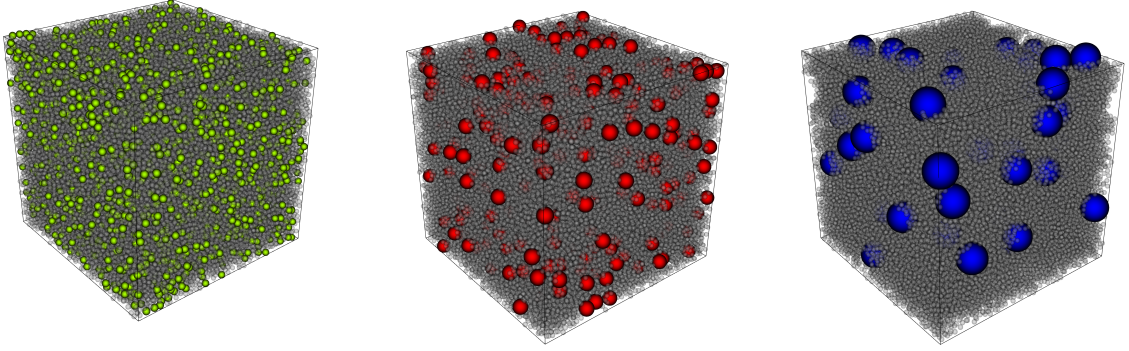


**Fig. 1:** Visualization of bidispersed dense suspensions at volume fraction  $\phi = 0.50$ , for different size of the larger particles dispersed (increasing from left to right). The grey colour shows the smaller particles, while the green, red and blue colours show the larger particles for the suspension with dispersion ratio  $\lambda = \{1.5, 3.0, 6.0\}$ , respectively. This colour-scheme will be used for referring to the different configurations throughout the whole manuscript.

software that models a dense, non-Brownian suspension (volume fraction  $\phi \geq 0.40$ ) of quasi-inertialess, neutrally-buoyant, rigid spherical particles in a shear-flow defined by the shear-rate  $\dot{\gamma}$ . The code tackles the Newton-Euler equations that govern the translational and rotational dynamics of the rigid particles,

$$\begin{cases} m_i \frac{d\mathbf{u}_i}{dt} \\ \mathbb{I}_i \frac{d\boldsymbol{\omega}_i}{dt} + \boldsymbol{\omega}_i \times (\mathbb{I}_i \boldsymbol{\omega}_i) \end{cases} = \sum_{j=1}^{N_H} \mathbf{F}_{ij}^H + \sum_{j=1}^{N_C} \mathbf{F}_{ij}^C + \sum_{j=1}^{N_E} \mathbf{F}_{ij}^E, \quad (1)$$

$$\sum_{j=1}^{N_H} \mathbf{T}_{ij}^H + \sum_{j=1}^{N_C} \mathbf{T}_{ij}^C + \sum_{j=1}^{N_E} \mathbf{T}_{ij}^E,$$

where the subscript  $i$  indicates the particle  $i \in [1, N]$ , being  $N$  the number of particles. The right-hand side of System (1) lists the forces and torques resulting from particle-flow and particle-particle interactions with the  $j$ th neighbour, and the superscripts  $H$ ,  $C$  and  $E$  indicate the nature of contribution, i.e. hydrodynamics, inelastic contacts and electro-chemical effects, respectively. The forces and torques are applied to the centre of mass of the  $i$ th particle, with mass  $m_i$  and inertia tensor  $\mathbb{I}_i$  and cause a variation in the translational and angular velocities of the particles, here denoted by the symbols  $\mathbf{u}_i$  and  $\boldsymbol{\omega}_i$ , respectively.

Next, we describe the models implemented for the three contributions listed above. Concerning the hydrodynamics of the system, dense

suspensions of rigid particles immersed in a low-Reynolds-number flow experience a Stokes drag and a pair-wise, short-range lubrication force [32], caused by the relative motion of near particles that squeezes the fluid flowing in the narrow gaps between them. The two contributions are implemented as a linear relationship between forces (torques) and velocities (angular velocities) [1, 32],  $\mathbf{F}^H = -\mathbb{R}(\mathbf{u} - \mathbf{U}^\infty)$ , where  $\mathbb{R}$  is a resistance matrix that is obtained by neglecting the far-field effects and considering only the dominant near-field divergent elements coming from the squeeze, shear and pump modes, following the work by Mari *et al.* [32].

The contact contribution is modelled with the stick-and-slide method [29]. This method mimics the inelastic contacts with spring-dashpot systems that start operating when two spheres overlap. The force can be expressed as  $\mathbf{F}^C = (k_n \delta + \gamma_n \dot{\delta}) \mathbf{n} + k_t \xi \mathbf{t}$ ; the spring-dashpot systems are oriented along the normal (centre-to-centre)  $\mathbf{n}$  and tangential  $\mathbf{t}$  directions (the latter to model the frictional component of the contacts) and are characterised by the spring and dashpot constants,  $(k_n, \gamma_n)$  and  $(k_t, \gamma_t = 0)$ , respectively, where the subscript indicate the direction ( $n$  normal and  $t$  tangential). The values  $\delta$  and  $\xi$  indicate the normal and tangential displacements of the springs and  $\dot{\delta}$  the normal projection of the overlapping velocity. The tangential contribution is subject to the Coulomb's law,  $|\mathbf{F}_t^C| \leq \mu |\mathbf{F}_n^C|$ , where  $\mu$  is

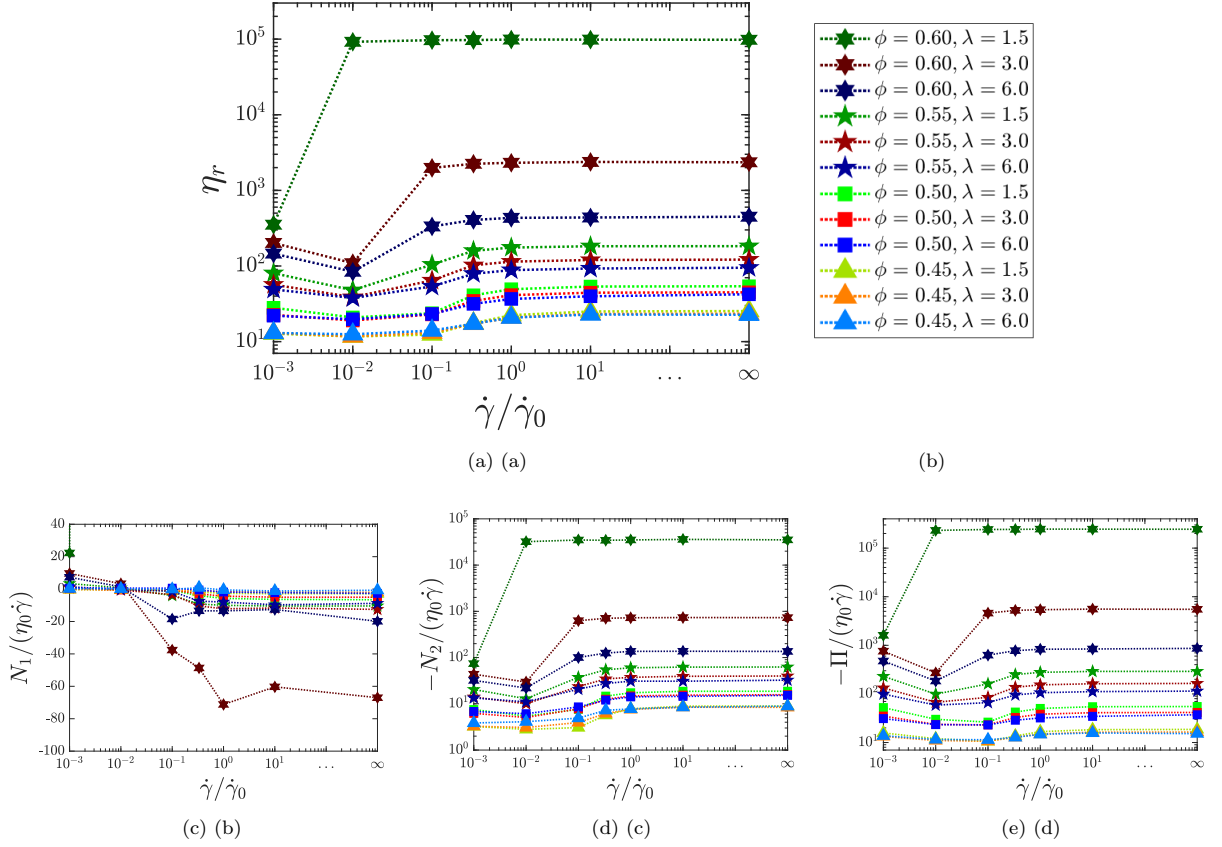


**Fig. 2:** Panel (a): Relative viscosity  $\eta_r$  as a function of the non-dimensional shear-rate  $\dot{\gamma}/\dot{\gamma}_0$ . Panel (b): First normal stress difference  $N_1/(\eta_0\dot{\gamma})$  as a function of the non-dimensional shear-rate  $\dot{\gamma}/\dot{\gamma}_0$ . The curve for the case  $(\phi = 0.60, \lambda = 1.5)$  largely exceeds the limits of the figure, reaching positive values of about  $N_1 \sim 8000$ , and are not shown to maintain the other curves visible. Panel (c): Second normal stress difference  $-N_2/(\eta_0\dot{\gamma})$  as a function of the non-dimensional shear-rate  $\dot{\gamma}/\dot{\gamma}_0$ . Panel (d): Pressure  $-\Pi/(\eta_0\dot{\gamma})$  as a function of the non-dimensional shear-rate  $\dot{\gamma}/\dot{\gamma}_0$ . In all the figures, the curves are obtained for suspensions at volume fraction  $\phi = \{0.45, 0.50, 0.55, 0.60\}$ , denoted by the triangle, square, star and star hexagon markers, respectively. The shades of green, red and blue represent the different dispersion ratio  $\lambda = \{1.5, 3.0, 6.0\}$ , as shown in figure 1. The markers and the colours are summarized within the legend shown in the top right of the figure.

the frictional coefficient. In this work, the friction coefficient is set to  $\mu = 0.5$  for all the scenarios analysed, as we did in a previous work where we compared our results with experimental data [41].

The last contribution considered in this work are forces that arise from the electrochemical properties of the suspension. These contributions are modelled as a sum of an inter-particle, distance-decaying repulsion force, and an attraction force in van der Waals form [17, 43],  $\mathbf{F}^E = \mathbf{F}^R + \mathbf{F}^A$ , where the superscripts  $E, R, A$  stand for

electrochemical, repulsive and attractive, respectively. The force resulting from the repulsive contribution can be written as  $\mathbf{F}^R = F_0 e^{-h/L_s} \mathbf{n}$ , where  $F_0$  is the magnitude of the force,  $L_s$  is the screening length and  $h$  is the particle-particle surface distance, while the attractive force can be written as  $\mathbf{F}^A = A\bar{a}/12(h^2 + \varepsilon^2) \mathbf{n}$ , where  $A$  is the Hamaker constant,  $\bar{a}$  is the harmonic mean radius of the two particles involved and  $\varepsilon$  is a smoothing term to eliminate the singularity when the two particles touch, i.e.  $h = 0$ .



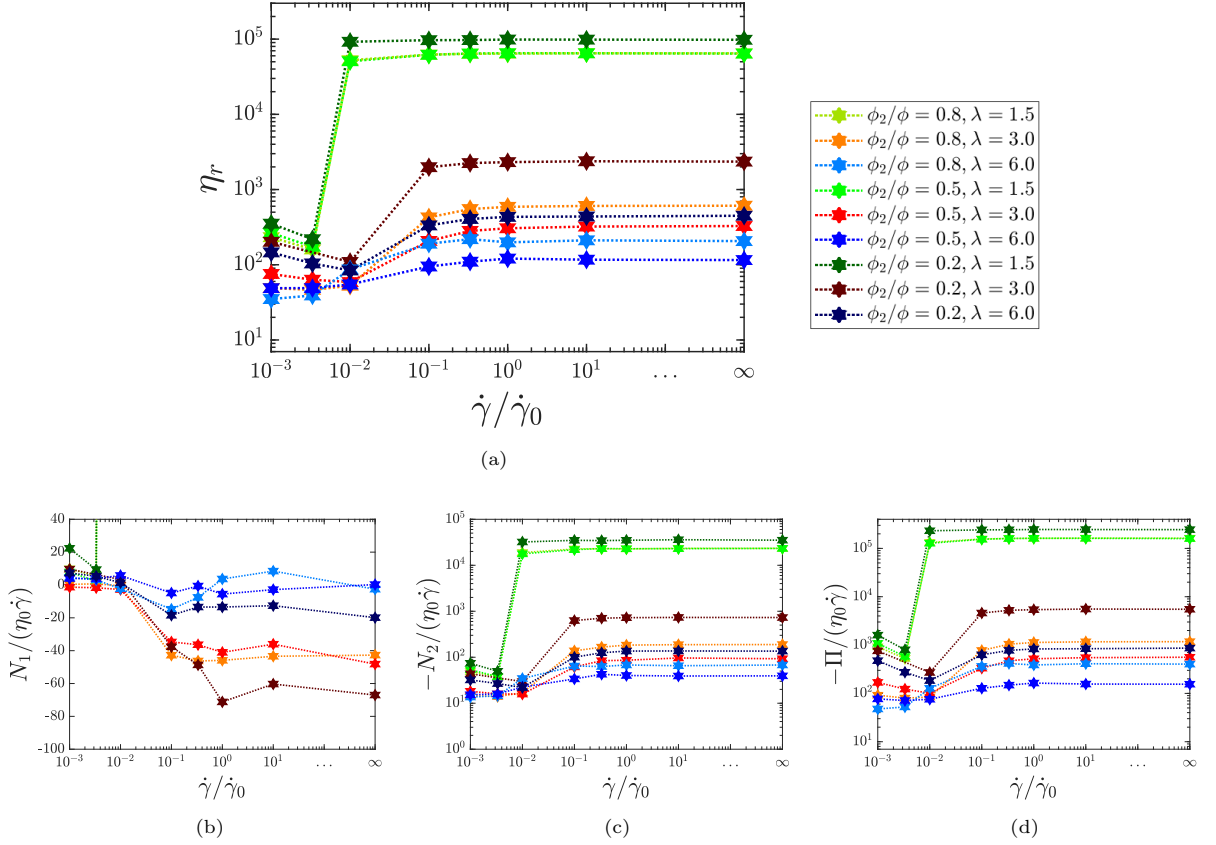


**Fig. 3:** Panel (a): Relative viscosity  $\eta_r$  as a function of the non-dimensional shear-rate  $\dot{\gamma}/\dot{\gamma}_0$ . Panel (b): First normal stress difference  $N_1/(\eta_0\dot{\gamma})$  as a function of the non-dimensional shear-rate  $\dot{\gamma}/\dot{\gamma}_0$ . The curve for the case ( $\phi = 0.60$ ,  $\lambda = 1.5$ ) largely exceeds the limits of the figure, reaching positive values of about  $N_1 \sim 8000$ , and are not shown to maintain the other curves visible. Panel (c): Second normal stress difference  $-N_2/(\eta_0\dot{\gamma})$  as a function of the non-dimensional shear-rate  $\dot{\gamma}/\dot{\gamma}_0$ . Panel (d): Pressure  $-\Pi/(\eta_0\dot{\gamma})$  as a function of the non-dimensional shear-rate  $\dot{\gamma}/\dot{\gamma}_0$ . In all the figures, the curves are obtained for suspensions at volume fraction  $\phi = 0.60$  (hexagon markers) varying the relative volume fractions of the dispersed phases, with  $\phi_2/\phi = \{0.2, 0.5, 0.8\}$ , from darker colours to lighter ones. The shades of green, red and blue represent the different dispersion ratio  $\lambda = \{1.5, 3.0, 6.0\}$ , as shown in figure 1. The markers and the colours are summarized within the legend shown in the top right of the figure.

Several parameters dominate the physics of the suspension described by the system of equations (1). Considering the translational equation of (1) and gathering the dimensional quantities, we can apply the Buckingham's  $\Pi$  theorem and find the set of the non-dimensional groups that can be tuned to outline the desired dynamics of the suspension. In particular, by choosing as independent fundamental quantities the scales that

define the hydrodynamics, the three following non-dimensional groups emerge: the Stokes number

$$St = \rho_p a_0^2 \dot{\gamma} / \eta_0, \quad (2)$$

that arises from the inertial term and compares the time-scale of the particles with the time-scale of the hydrodynamics. In the equation above,  $\rho_p$  is the density of the particles (equal to the density of the carrier fluid in the cases we considered),  $a_0$  is the typical length scale of the system (the

radius of the particles of the smallest phase of the suspension),  $\eta_0$  is the viscosity of the carrier fluid and  $\dot{\gamma}$  is the shear-rate applied to the suspension. The constraint  $St \ll 1$  is applied to enforce the inertialess regime. The second number is the non-dimensional stiffness

$$\hat{k} = k_n/(\eta_0 a_0 \dot{\gamma}), \quad (3)$$

that weighs the importance of the contacts contributions compared to the hydrodynamic term. In this case, the constraint  $\hat{k} \gg 1$  is set to force the particles to be rigid. We considered the normal spring constant  $k_n$  as the dominant term of the spring-dashpot systems since we enforce the additional constraints  $k_t = 2/7 k_n$  and  $\gamma_n \dot{\gamma}/k_n \ll 1 \sim O(10^{-7})$ , where the latter is the relaxation time of the spring-dashpot system. Finally, the last non-dimensional group, i.e. the equivalent shear-rate

$$\hat{\gamma} = |\mathbf{F}^E(d_{ij} = 0)|/(\eta_0 a_0^2 \dot{\gamma}) = \dot{\gamma}_0/\dot{\gamma}, \quad (4)$$

refers to the time-scale introduced by the electrochemical contribution and is tuned to set a shear-rate dependent rheology on the suspension. Here  $d_{ij}$  is the relative surface-surface distance between the particles  $i$  and  $j$ .

More details can be found in our previous publication Monti et al. [36], together with validations against theory, numerical simulations and experimental measurements. The software can be freely downloaded at the following link <https://github.com/marco-rosti/CFF-Ball-0x>.

### 3 Results

We start the analysis by looking at the rheological properties of the suspensions. Panel (a) of figure 2 shows the flow curve of the suspension, i.e. how the relative viscosity  $\eta_r$  of the suspension varies with the applied shear rate  $\dot{\gamma}/\dot{\gamma}_0$ . The curves are grouped using the markers to distinguish the different volume fractions analyzed (triangles:  $\phi = 0.45$ ; squares:  $\phi = 0.50$ ; stars:  $\phi = 0.55$ ; star hexagons:  $\phi = 0.60$ ) and the colours to discriminate the dispersion ratio, in accordance with figure 1 (green:  $\lambda = 1.5$ ; red:  $\lambda = 3.0$ ; blue:  $\lambda = 6.0$ ). This is recapped in the legend of figure 2. All the curves plotted show a shear-thinning region

followed by the a Newtonian plateau at low shear-rates, followed by a region of viscosity increase, i.e. the shear-thickening regime, and a final plateau at high shear rates. We observe that the presence of large particles reduces, at high shear-rates, the relative viscosity of the suspension and weakens its shear-thickening behaviour: thus, we find that a bidispersed suspension with large dispersion ratio exhibit CST where an equivalent suspension (with same volume fraction) of monodispersed particles would have an abrupt change of the rheological properties, e.g. DST. The effect of the dispersion ratio is enhanced for large volume fractions, as getting closer to the jamming. These findings are consistent with those by D’Haene and Mewis [12], but different from those by Madraki et al. [30, 31]. A possible explanation of this discrepancy has to be traced back to the increase of the total volume fraction of the suspension in the latter [30, 31].

When studying the rheology of a suspension, the two independent normal stress differences must be considered, along with the viscosity. The values obtained by the numerical simulations of these quantities together with the pressure are shown in figure 2, panels (b)–(d), where panel (b) shows the first normal stress difference  $N_1 = \Sigma_{11} - \Sigma_{33}$ , panel (c) the second normal stress difference  $N_2 = \Sigma_{22} - \Sigma_{33}$ , and panel (d) the pressure  $\Pi = \text{Tr}(\Sigma)/3$ ; in the definition of the rheological quantities,  $\Sigma$  represents the stress-tensor computed by means of the stresslet theory [18]. The three rheological quantities are shown for all the cases studied in this work. Overall, we observe that the first normal stress difference is small and dominated by fluctuations, as already observed by other authors [32, 43]. The second normal stress difference is always negative and its absolute value exhibit a trend similar to the pressure and relative viscosity, consistently to the ones observed in the literature [32]. The effect of the dispersion ratio for these two quantities, closely reflects the behaviour shown by the relative viscosity, with the exception of the first normal stress difference which suddenly changes sign and strongly increases by several orders of magnitude when the suspension undergoes DST.

After that, we picked the most interesting case in terms of rheological properties, i.e.  $\phi = 0.60$  where  $\lambda$  affects DST ( $\lambda = 1.5$ ) by weakening it to CST ( $\lambda = \{3.0, 6.0\}$ ), and we analysed the trends of the relative viscosity, normal stress differences

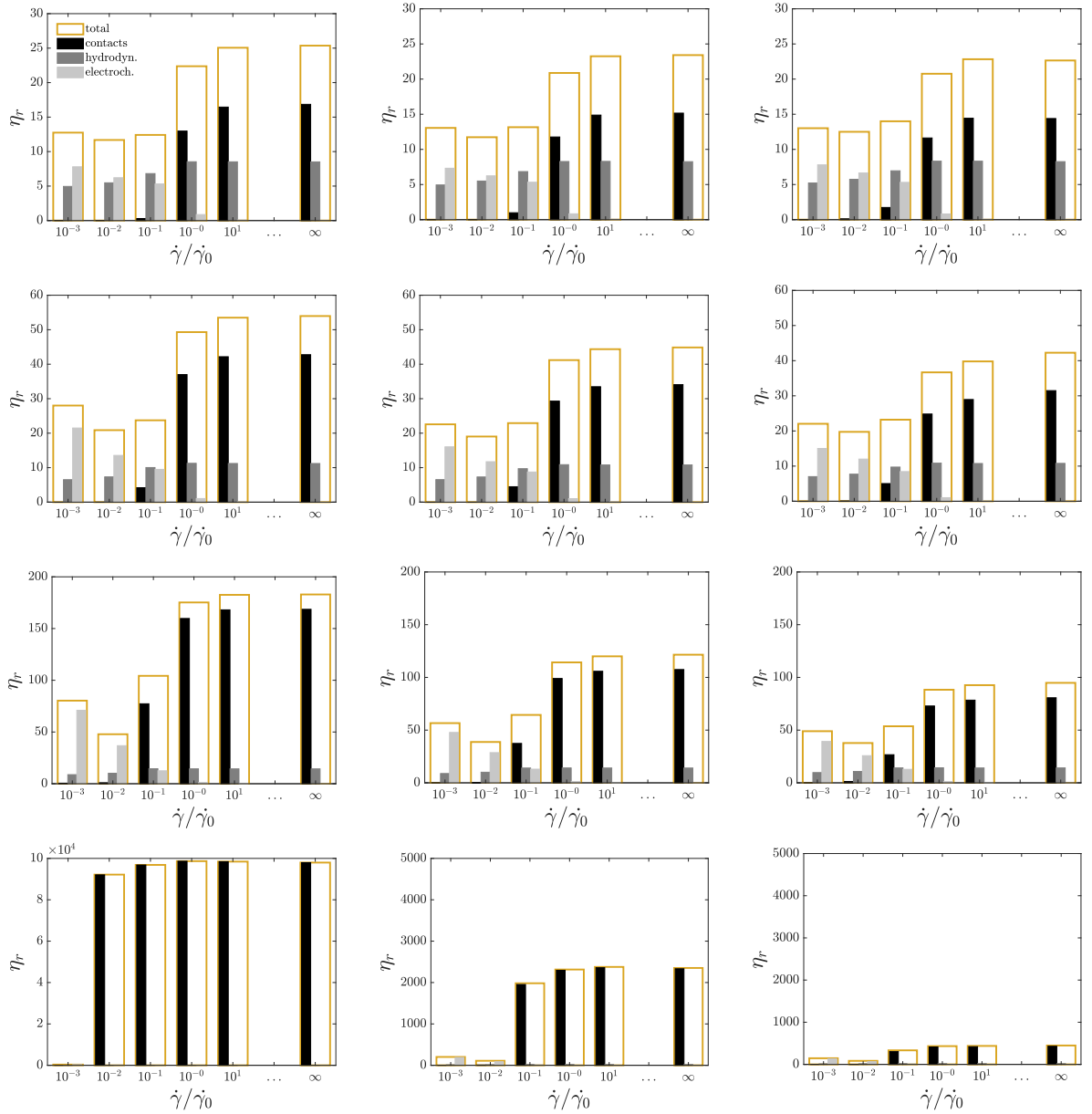


**Fig. 4:** Contributions to the relative viscosity  $\eta_r$  of the contacts (black), hydrodynamics (darker grey) and electrochemical potentials (lighter grey), as a function of the non-dimensional shear-rate  $\dot{\gamma}/\dot{\gamma}_0$ . The suspensions represented have increasing volume fractions from the top row ( $\phi = 0.45$ ) to the bottom row ( $\phi = 0.60$ ) and increasing dispersion ratio,  $\lambda = \{1.5, 3.0, 6.0\}$ , from left to right. Note that, in the last row, the bars in the left panel are on a different scale compared with the bars in the central and right panels.

and pressure varying the relative volume fraction of the dispersed phase, i.e.  $\phi_2/\phi = \{0.2, 0.5, 0.8\}$ . As per [figure 2](#), panel (a) of [figure 3](#) shows the flow curve of the suspension, i.e. how the relative viscosity  $\eta_r$  of the suspension varies with the

applied shear rate  $\dot{\gamma}/\dot{\gamma}_0$ . The curves are grouped using the colours to discriminate the dispersion ratio, in accordance with [figure 1](#) (green:  $\lambda = 1.5$ ; red:  $\lambda = 3.0$ ; blue:  $\lambda = 6.0$ ) and the shades of the colours to identify the relative volume fractions

analysed, with colours going from light to dark for increasing  $\phi_2/\phi$ . This is recapped in the legend of [figure 3](#) (note that the curves  $\phi_2/\phi = \{0.5, 0.8\}$  at  $\lambda = 1.5$  almost overlap). The curves show, as in [figure 2](#), a shear-thinning region followed by the Newtonian plateau at low shear-rates, followed by a region of viscosity increase, i.e. the shear-thickening regime, and a final plateau at high shear rates. The effect of the relative volume fractions controls the relative viscosity, reducing it when the two phases have similar volume fractions and increasing it when the dispersion tends towards the monodispersion. For the cases with  $\phi_2/\phi = \{0.2, 0.8\}$ , consistently with the previous works [[7–9](#), [20](#), [39](#)], the relative viscosity is higher when there are more smaller particles than larger ones immersed in the suspension. Even in this case, we observe that the relative volume fraction can reduce, at high shear-rates, the relative viscosity of the suspension and weakens its shear-thickening behaviour, especially when  $\phi_2 = \phi_1$ . However, the effect of the relative volume fraction does not have a strong impact as the the relative size of the dispersed phases.

The normal stresses of these suspensions, instead, are shown in [figure 3](#), panels (b)–(d), where panel (b) shows the first normal stress difference  $N_1 = \Sigma_{11} - \Sigma_{33}$ , panel (c) the second normal stress difference  $N_2 = \Sigma_{22} - \Sigma_{33}$ , and panel (d) the pressure  $\Pi = \text{Tr}(\Sigma)/3$ , as in [figure 2](#); in the definition of the rheological quantities,  $\Sigma$  represents the stress-tensor computed by means of the stresslet theory [[18](#)]. The three rheological quantities are shown for all the pairs of relative volume fractions  $(\phi_1, \phi_2)$  at  $\phi = 0.60$  studied in this work. We observe that the first normal stress difference is small and still dominated by fluctuations. Once more, the second normal stress difference is always negative and its absolute value exhibit a trend similar to the pressure and relative viscosity, consistently to the ones observed in the literature [[32](#)]. The effect of the relative volume fractions of the two phases reflects the behaviour shown by the relative viscosity, with the exception of the first normal stress, similarly to what has been observed in [figure 2](#).

In order to highlight the origin of the reduced relative viscosity of the suspension with increasing dispersion ratio of the particles, we separate the contributions to the total stress accounted

by the contacts, hydrodynamics and electrochemical potentials. In particular, [figure 4](#) shows the contributions to the relative viscosity for the suspensions at different dispersion ratios. [Figure 4](#) is structured in a  $4 \times 3$  matrix of panels, where each row of the matrix shows the contributions to the relative viscosity for increasing volume fractions ( $\phi$  increases from top to bottom), while each column shows the effect for different dispersion ratios ( $\lambda$  increases from left to right). In each panel of the figure, we report the contribution to the total relative viscosity (golden lines) of the contacts (black bars), hydrodynamics (darker grey) and electrochemical potentials (lighter grey), as a function of the shear-rate. [Figure 4](#) reveals that, at low shear rates (left end of each panel), the suspension rheology is dominated by the electrochemical potentials, with a little contribution due to the hydrodynamics and a null contribution of the contacts. On the other hand, at high shear-rates (right end of each panel), the hydrodynamics has a small, almost shear-independent, contribution and the electrochemical potentials play no role, as expected; the contacts dominate the rheology of the suspension at these shear-rates, in agreement with the theory that relates shear-thickening and (frictional) contacts, recently proposed and experimentally proved [[14](#), [27](#), [32](#), [33](#), [42](#)]. [Figure 4](#) shows that, while the hydrodynamics remains constant in the shear-thickening regime and the consequent plateau, the contribution of the contacts drops when increasing the size of the larger phase dispersed. This phenomenon becomes more evident when dealing with larger volume fractions, where DST can be reduced to CST by simply adding larger particles (see the last row of panels of [figure 4](#)). This provides a quantitative explanation of the behaviour observed in the flow curves of [figure 2](#).

The reduction of contacts we observed for large values of  $\lambda$ , which is the origin of the lower relative viscosity, can be explained geometrically as a reduced total surface area of the suspension in the case with high dispersion ratios. Indeed, as  $\lambda$  grows, the total surface area  $A = \pi a_1^2(n_1 + n_2\lambda^2)$  monotonically decreases when the total volume fraction  $\phi$  is kept constant (together with the relative volume fractions of the two phases that establish a non-linear dependency of  $n_1$  and  $n_2$  on  $\lambda$ ). In other terms, for a given volume fraction of the dispersed phases, the area available

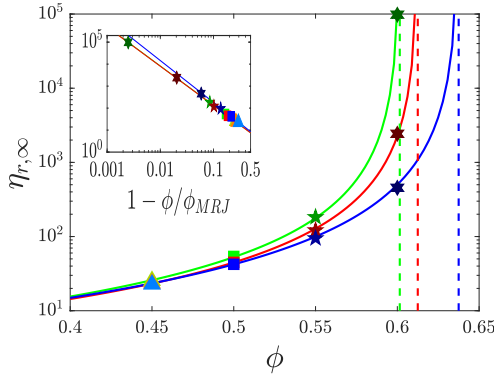


**Fig. 5:** Relative viscosity in the high shear-rate limit,  $\eta_{r,\infty} = \eta_r(\dot{\gamma}/\dot{\gamma}_0 \rightarrow \infty)$ , as a function of the volume fraction  $\phi$ . The colour of the curves and the style of the markers reflect the ones used in figure 2. The solid lines are obtained from fitting the data available with power-laws  $\eta_{r,\infty} = \alpha(1 - \phi/\phi_{MRJ})^{-\beta}$  (as shown in the inset) and the dashed lines correspond to the values of  $\phi_{MRJ}$  obtained for the three configurations of suspensions considered. The best fitting parameters are  $(\phi_{MRJ}, \alpha, \beta)_{\lambda=1.5} = (0.6015, 2.20, 1.79)$ ,  $(\phi_{MRJ}, \alpha, \beta)_{\lambda=3.0} = (0.6125, 2.18, 1.79)$ ,  $(\phi_{MRJ}, \alpha, \beta)_{\lambda=6.0} = (0.6375, 2.28, 1.90)$ .

for contacts among particles is smaller for larger  $\lambda$ , thus reducing the probability of having contacts between the particles. Note that this is valid only for spheres. This result is confirmed by the coordination number defined as  $N_c = 4\pi \int_0^{\bar{r}/a_0} r^2 g(r) N/V dr$ , where  $r$  is the distance from the origin,  $V$  is the volume of the computational box, and  $g(r)$  is the radial distribution function. Here,  $\bar{r}/a_0 = 20$  is used to take into account the large dispersion ratio. The coordination number is an indicator of the average number of collisions between particles. We computed  $N_c$  for all the dispersion ratios of the suspensions at  $\phi = 60$  shown in figure 5 and, to emphasize the results, we normalised  $N_c$  by the coordination number of the case with  $\lambda = 1.5$ . Thus, we obtain  $N_c = [1, 0.859, 0.856]$  for  $\lambda = [1.5, 3.0, 6.0]$ . As for the relative viscosity and the total surface area  $A$ , the coordination number shows a decreasing trend with  $\lambda$ . More quantitatively, the change of  $A$  with  $\lambda$  modifies the properties of the packing of the suspension as demonstrated by Hopkins *et al.* [21, 22]. In particular, it was shown that

the increase of the dispersion ratio  $\lambda$  enhances the efficiency of the packing, resulting in an increase of  $\phi_{MRJ}$ . This geometrically constraint affects the rheological properties of the suspension when it approaches the jamming transition, i.e., when the contacts dominate the rheology. In this case, the relative viscosity  $\eta_r$  can be expressed as a power law diverging for  $\phi \rightarrow \phi_{MRJ}$ , i.e.,  $\eta_r \sim (1 - \phi/\phi_{MRJ})^{-\beta}$  [4, 15, 32]. We show this by considering the relative viscosity in the high shear-rate limit as a function of the volume fraction  $\eta_{r,\infty}(\phi) = \eta_r(\phi, \dot{\gamma}/\dot{\gamma}_0 \rightarrow \infty)$ , see figure 5, where the plotted curves have been obtained by fitting our numerical data with a power-law of the form  $\eta_{r,\infty} = \alpha(1 - \phi/\phi_{MRJ})^{-\beta}$ , as shown in the inset of the same figure [32]. Figure 5 proves that  $\phi_{MRJ}$  grows with  $\lambda$ , and thus explains that the differences in the values of the relative viscosity, previously observed at the beginning of this work for the different dispersion ratios (figure 2), is a direct consequence of the variation of the packing efficiency which determines the infinite shear-rate limit of  $\eta_r$  to be achieved after the shear-thickening region.

## 4 Conclusion

In this work, we studied the rheological behaviour of bidispersed suspensions of non-Brownian spherical particles, and we showed that the presence of a large dispersed phase reduces the shear-thickening behaviour of the suspension. This phenomenon is caused by the more efficient maximally random jammed packing exhibited by the suspensions with large dispersion ratio, that results in a reduction of contacts and thus of their contribution to the relative viscosity of the suspension. We also studied the effect of the relative volume fractions of the dispersed phases and we found that a lower viscosity is achieved when the dispersed phases have similar (identical in our work) volumes, coherently with the results already discussed in the literature. The effect of the latter parameter on the rheological properties of the suspensions, however, is not as important as the bidispersion ratio. The results discussed here are of particular interests as a simple control strategy for the rheology of particle suspensions, especially in their shear-thickening regime, with direct impact on the flowability of the complex material. Indeed, it is possible to force the transition from DST to CST (or vice-versa) by



simply substituting a partial volume fraction of a monodispersed suspension, with an equivalent one of large (or small) particles.

**Acknowledgments.** All authors gratefully acknowledge the support of Okinawa Institute of Science and Technology Graduate University (OIST) with subsidy funding from the Cabinet Office, Government of Japan. The authors also acknowledge the computer time provided by the Scientific Computing section of Research Support Division at OIST.

## Competing Interests

The authors have no competing interests to disclose.

## References

- [1] Ball, R. and Melrose, J. R. (1997). A simulation technique for many spheres in quasi-static motion under frame-invariant pair drag and brownian forces. *Physica A: Statistical Mechanics and its Applications*, 247(1-4):444–472.
- [2] Barnes, H. (1989). Shear-thickening (“dilatancy”) in suspensions of nonaggregating solid particles dispersed in newtonian liquids. *Journal of Rheology*, 33(2):329–366.
- [3] Bender, J. and Wagner, N. J. (1996). Reversible shear thickening in monodisperse and bidisperse colloidal dispersions. *Journal of Rheology*, 40(5):899–916.
- [4] Boyer, F., Guazzelli, É., and Pouliquen, O. (2011). Unifying suspension and granular rheology. *Physical review letters*, 107(18):188301.
- [5] Brown, E. and Jaeger, H. M. (2009). Dynamic jamming point for shear thickening suspensions. *Physical review letters*, 103(8):086001.
- [6] Brown, E. and Jaeger, H. M. (2011). Through thick and thin. *Science*, 333(6047):1230–1231.
- [7] Chang, C. and Powell, R. (1993). Dynamic simulation of bimodal suspensions of hydrodynamically interacting spherical particles. *Journal of Fluid Mechanics*, 253:1–25.
- [8] Chang, C. and Powell, R. (1994a). The rheology of bimodal hard-sphere dispersions. *Physics of Fluids*, 6(5):1628–1636.
- [9] Chang, C. and Powell, R. L. (1994b). Self-diffusion of bimodal suspensions of hydrodynamically interacting spherical particles in shearing flow. *Journal of Fluid Mechanics*, 281:51–80.
- [10] Clavaud, C., Bérut, A., Metzger, B., and Forterre, Y. (2017). Revealing the frictional transition in shear-thickening suspensions. *Proceedings of the National Academy of Sciences*, 114(20):5147–5152.
- [11] Cwalina, C. D. and Wagner, N. J. (2016). Rheology of non-brownian particles suspended in concentrated colloidal dispersions at low particle reynolds number. *Journal of Rheology*, 60(1):47–59.
- [12] D’Haene, P. and Mewis, J. (1994). Rheological characterization of bimodal colloidal dispersions. *Rheologica acta*, 33(3):165–174.
- [13] Donev, A., Torquato, S., Stillinger, F. H., and Connelly, R. (2004). Jamming in hard sphere and disk packings. *Journal of applied physics*, 95(3):989–999.
- [14] Fernandez, N., Mani, R., Rinaldi, D., Kadau, D., Mosquet, M., Lombois-Burger, H., Cayer-Barrioz, J., Herrmann, H. J., Spencer, N. D., and Isa, L. (2013). Microscopic mechanism for shear thickening of non-brownian suspensions. *Physical review letters*, 111(10):108301.
- [15] Forterre, Y. and Pouliquen, O. (2008). Flows of dense granular media. *Annu. Rev. Fluid Mech.*, 40:1–24.
- [16] Freundlich, H. and Röder, H. (1938). Dilatancy and its relation to thixotropy. *Transactions of the Faraday Society*, 34:308–316.
- [17] Gálvez, L., de Beer, S., van der Meer, D., and Pons, A. (2017). Dramatic effect of fluid chemistry on cornstarch suspensions: Linking particle interactions to macroscopic rheology. *Physical Review E*, 95(3):030602.

- [18] Guazzelli, E. and Morris, J. (2011). *A physical introduction to suspension dynamics*, volume 45. Cambridge University Press.
- [19] Guy, B., Hermes, M., and Poon, W. C. (2015). Towards a unified description of the rheology of hard-particle suspensions. *Physical review letters*, 115(8):088304.
- [20] Guy, B. M., Ness, C., Hermes, M., Sawiak, L. J., Sun, J., and Poon, W. C. (2020). Testing the wyart–cates model for non-brownian shear thickening using bidisperse suspensions. *Soft Matter*, 16(1):229–237.
- [21] Hopkins, A. B., Stillinger, F. H., and Torquato, S. (2012). Densest binary sphere packings. *Physical Review E*, 85(2):021130.
- [22] Hopkins, A. B., Stillinger, F. H., and Torquato, S. (2013). Disordered strictly jammed binary sphere packings attain an anomalously large range of densities. *Physical Review E*, 88(2):022205.
- [23] Hsu, C.-P., Ramakrishna, S. N., Zanini, M., Spencer, N. D., and Isa, L. (2018). Roughness-dependent tribology effects on discontinuous shear thickening. *Proceedings of the National Academy of Sciences*, 115(20):5117–5122.
- [24] Jamali, S. and Brady, J. (2019). Alternative frictional model for discontinuous shear thickening of dense suspensions: Hydrodynamics. *Physical review letters*, 123(13):138002.
- [25] Jamali, S., Yamanoi, M., and Maia, J. (2013). Bridging the gap between microstructure and macroscopic behavior of monodisperse and bimodal colloidal suspensions. *Soft Matter*, 9(5):1506–1515.
- [26] Lerner, E., Düring, G., and Wyart, M. (2012). A unified framework for non-brownian suspension flows and soft amorphous solids. *Proceedings of the National Academy of Sciences*, 109(13):4798–4803.
- [27] Lin, N. Y., Guy, B. M., Hermes, M., Ness, C., Sun, J., Poon, W. C., and Cohen, I. (2015). Hydrodynamic and contact contributions to continuous shear thickening in colloidal suspensions. *Physical review letters*, 115(22):228304.
- [28] Lin, N. Y., Ness, C., Cates, M. E., Sun, J., and Cohen, I. (2016). Tunable shear thickening in suspensions. *Proceedings of the National Academy of Sciences*, 113(39):10774–10778.
- [29] Luding, S. (2008). Cohesive, frictional powders: contact models for tension. *Granular matter*, 10(4):235.
- [30] Madraki, Y., Hormozi, S., Ovarlez, G., Guazzelli, E., and Pouliquen, O. (2017). Enhancing shear thickening. *Physical Review Fluids*, 2(3):033301.
- [31] Madraki, Y., Ovarlez, G., and Hormozi, S. (2018). Transition from continuous to discontinuous shear thickening: An excluded-volume effect. *Physical review letters*, 121(10):108001.
- [32] Mari, R., Seto, R., Morris, J. F., and Denn, M. M. (2014). Shear thickening, frictionless and frictional rheologies in non-brownian suspensions. *Journal of Rheology*, 58(6):1693–1724.
- [33] Mari, R., Seto, R., Morris, J. F., and Denn, M. M. (2015). Discontinuous shear thickening in brownian suspensions by dynamic simulation. *Proceedings of the National Academy of Sciences*, 112(50):15326–15330.
- [34] Melrose, J., Van Vliet, J., and Ball, R. (1996). Continuous shear thickening and colloid surfaces. *Physical review letters*, 77(22):4660.
- [35] Mewis, J. and Wagner, N. J. (2012). *Colloidal suspension rheology*. Cambridge university press.
- [36] Monti, A., Rathee, V., Shen, A. Q., and Rosti, M. E. (2021). A fast and efficient tool to study the rheology of dense suspensions. *Physics of Fluids*, 33(10):103314.
- [37] More, R. V. and Ardekani, A. M. (2020). Effect of roughness on the rheology of concentrated non-brownian suspensions: A numerical study. *Journal of Rheology*, 64(1):67–80.

- [38] Ozturk, D., Morgan, M. L., and Sandnes, B. (2020). Flow-to-fracture transition and pattern formation in a discontinuous shear thickening fluid. *Communications Physics*, 3(1):1–9.
- [39] Pednekar, S., Chun, J., and Morris, J. F. (2018). Bidisperse and polydisperse suspension rheology at large solid fraction. *Journal of Rheology*, 62(2):513–526.
- [40] Pradeep, S., Nabizadeh, M., Jacob, A. R., Jamali, S., and Hsiao, L. C. (2021). Jamming distance dictates colloidal shear thickening. *Physical Review Letters*, 127(15):158002.
- [41] Rathee, V., Monti, A., Rosti, M. E., and Shen, A. Q. (2021). Shear thickening behavior in dense repulsive and attractive suspensions of hard spheres. *Soft Matter*, 17(35):8047–8058.
- [42] Seto, R., Mari, R., Morris, J. F., and Denn, M. M. (2013). Discontinuous shear thickening of frictional hard-sphere suspensions. *Physical review letters*, 111(21):218301.
- [43] Singh, A., Pednekar, S., Chun, J., Denn, M. M., and Morris, J. F. (2019). From yielding to shear jamming in a cohesive frictional suspension. *Physical review letters*, 122(9):098004.
- [44] Torquato, S., Truskett, T. M., and Debenedetti, P. G. (2000). Is random close packing of spheres well defined? *Physical review letters*, 84(10):2064.
- [45] Wagner, N. J. and Brady, J. F. (2009). Shear thickening in colloidal dispersions. *Physics Today*, 62(10):27–32.
- [46] Wyart, M. and Cates, M. E. (2014). Discontinuous shear thickening without inertia in dense non-brownian suspensions. *Physical review letters*, 112(9):098302.